Supporting Information

Low-fouling CNT-PEG-hydrogel-coated quartz crystal microbalance sensor for saliva glucose detection

Shiwen Wang,[ab] Guanjiang Liu,[b] Bei Yang,[b] Zifeng Zhang,[b] Debo Hu,[b]Chenchen Wu,[b] Yaling Qin,[b] Qian Dou, *[b] Wenping Hu*[a]

[a.] Tianjin Key Laboratory of Molecular Optoelectronic Sciences, Department of Chemistry, School of Sciences, Tianjin University, Tianjin, 300072, China

[b.] CAS Key Laboratory of Nanophotonic Materials and Devices, CAS Key Laboratory of Standardization and Measurement for Nanotechnology, CAS Center for Excellence in Nanoscience, National Center for Nanoscience and Technology, Beijing 100190, China

E-mail: huwp@tju.edu.cn; douq@nanoctr.cn.Tel: +86-010-82545720

Recognition mechanism

The CNT-PEG-hydrogel film consists of two layers: the top CNT-PEG layer provides channels for transporting glucose molecules and filters macromolecular impurities and the bottom base PBA-hydrogel film which provide the glucose binding sites.

When the glucose molecules contract with the CNT-PEG-hydrogel film, the holes of CNT-PEG layer displayed 5~10 nm that provided adequate pathways and permit glucose molecules (the diameter is 0.36 nm) to transfer.[1]At the meantime, the CNT-PEG layer could improve the aqueous surface wettability and form a stable hydration layer, which is beneficial for resisting protein adsorption and improving the diffusion of soluble glucose through to PBA-hydrogel.

Phenylboronic acid (PBA) and its derivatives are the most widely used artificial compounds for fabrication of glucose-responsive units. PBA groups are in equilibrium between a negatively charged dissociated state and an uncharged non-dissociated state **(Fig. S1)**.[1] Non-dissociated PBA is a flat triangle and forms an unstable complex with glucose, while dissociated PBA has a tetrahedral structure and can form cyclic lactones with glucose molecules via the reversible interaction of diol-containing glucose molecules and hydroxyl group of dissociated PBA.[2, 3]

The QCM sensor has been employed as a highly sensitive mass detector, which allows the measurement of in situ changes in mass with nanogram resolution. When

voltage is applied to a quartz crystal causing it to oscillate at a specific frequency, the change in mass on the quartz surface is related to the change in frequency of the oscillating crystal. Therefore, when the glucose molecules react with CNT-PEG-hydrogel coated quartz crystals that will cause the mass increased and resonance frequency will be decreased **(Fig. S1b)**.

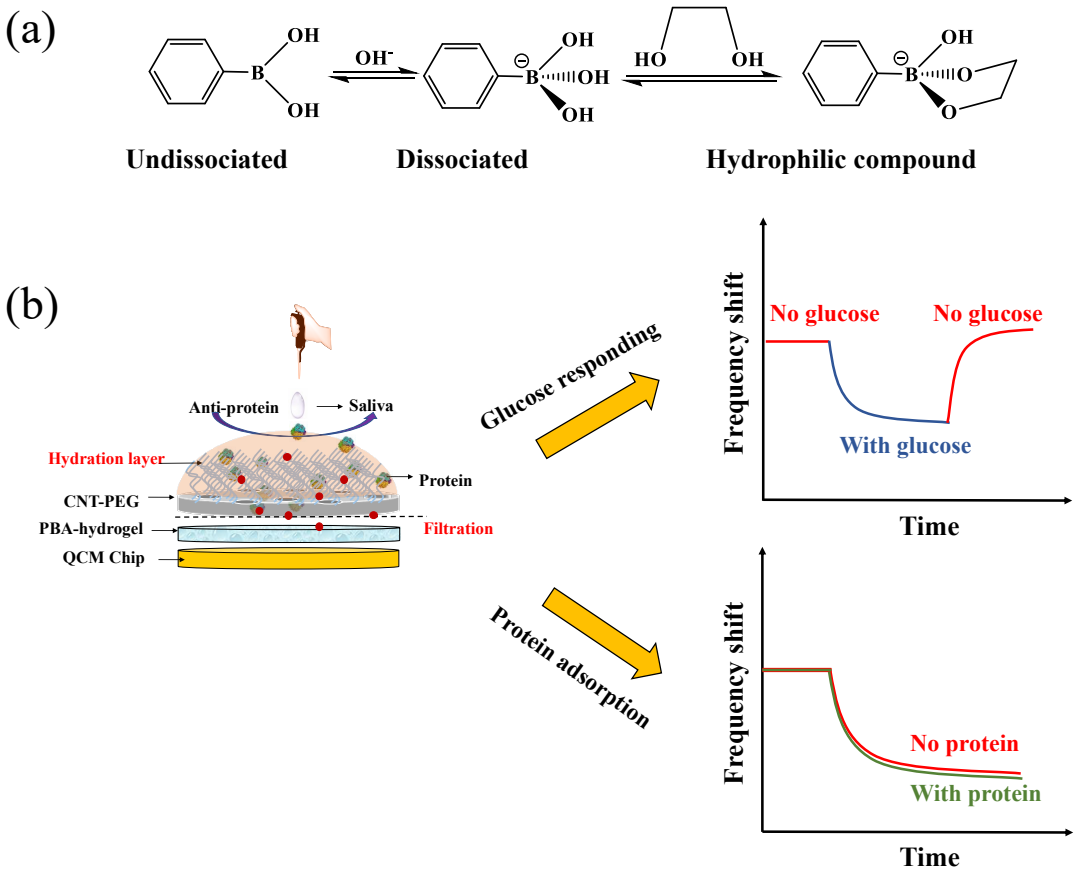

Fig. S1 (a) The mechanism of glucose recognition between PBA-hydrogel and glucose molecules. (b) The CNT-PEG-hydrogel coated-QCM chip can effectively recognize the glucose molecules and resist the non-specific adsorption of proteins.

The AFM images of PBA-hydrogel and CNT-PEG-hydrogel

The AFM images showed smooth and homogenous coverage with the PBA-hydrogel film without any uncovered areas (**Fig. S2a**). The roughness (root mean square) of the surface was Rms = 3.99 ± 1.08 nm. After CNT-PEG coating onto the surface of the PBA-hydrogel film, the surface appeared uneven and CNT-PEG

staggered on the surface of hydrogel, the surface roughness will be increased to Rms = 44.06 ± 14.4 nm (Fig. S2b).

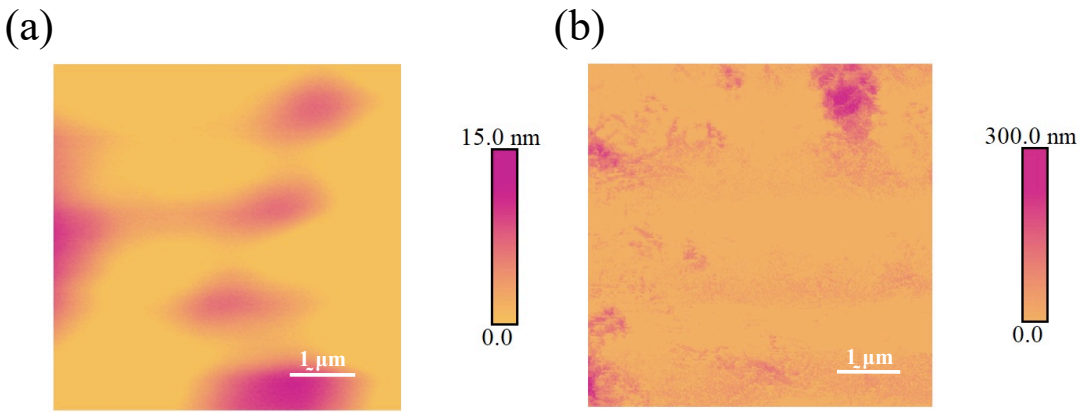

Fig. S2 A topographical image of the PBA-hydrogel film (a) and CNT-PEG-hydrogel film (b).

X-ray photoelectron spectroscopy (XPS)

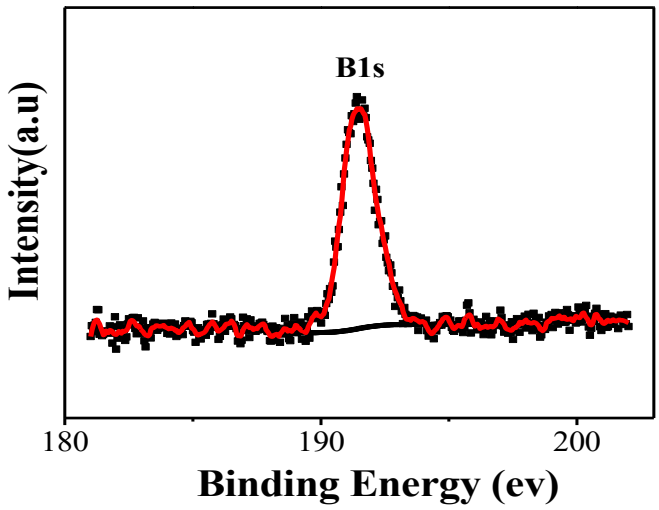

Fig. S3 High resolution B1s XPS spectra of CNT-PEG-hydrogel was immobilized on the QCM sensor surface

Table S1 Elemental surface composition of CNT-COOH, CNT-PEG, PBA-hydrogel and CNT-PEG-hydrogel film determined from XPS

Element (atom %)	CNT-COOH	CNT-PEG	PBA-hydrogel	CNT-PEG-hydrogel
C	91.635	90.335	69.506	68.87
O	6.903	8.411	16.388	17.322
N	1.238	0.441	11.642	12.019
B	–	–	2.123	1.789
S	0.225	0.813	0.341	–

FTIR spectra

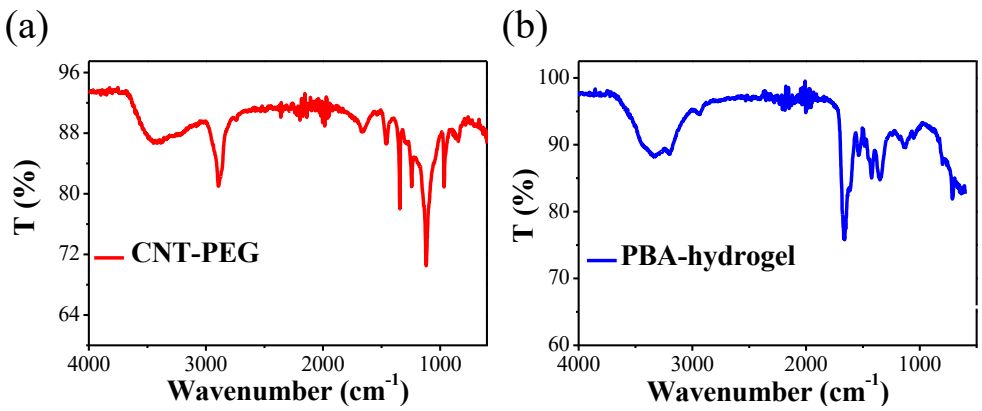

Fig. S4 FTIR spectra of CNT-PEG nanotubes (a) and PBA-hydrogel films (b).

Reproducibility of PBA-hydrogel and CNT-PEG-hydrogel in the PBS

The stability of the PBA-hydrogel and CNT-PEG-hydrogel film-coated QCM sensor were evaluated, based on the repeated detection of glucose at constant glucose concentration (0 and 50 mg/L) at pH=7.5. Table S2. shows that the relative standard deviations (RSD) are less than 10%, indicating that the PBA-hydrogel and CNT-PEG-hydrogel film-coated QCM sensor have good reproducibility.

Table. S2 The % RSD of PBA-hydrogel film and CNT-PEG-hydrogel after five association-dissociation cycles.

Film	PBA-hydrogel	CNT-PEG-hydrogel
Glucose level (mg/L)	50	
Delta F(Hz)	-33.0	-46.4
	-31.6	-48.1
	-30.7	-50.2
	-30.1	-49.7
	-31.2	-52.8
Mean response (Hz)	-31.3	-49.4
Standard deviations	1.0	2.4
RSD	3.2%	4.9%

The reproducibility of CNT-PEG-hydrogel film-coated QCM sensors in 10% saliva.

The reproducibility of the CNT-PEG-hydrogel film-coated QCM sensor was evaluated based on the repeated detection of glucose for 5 times at constant glucose concentration 50 mg/L, 100 mg/L, 200 mg/L, respectively, in 10% saliva. Table S2. shows that the relative standard deviations (RSD) are approach to 10%, indicating that CNT-PEG-hydrogel film-coated QCM sensor has a good reproducibility in 10% saliva.

Table S3. The reproducibility of the CNT-PEG-hydrogel film-coated QCM sensors in 10% saliva.

CNT-PEG-hydrogel			
Glucose level (mg/L)	50	100	200
	-65.7	-154.0	-254.3
	-67.3	-188.2	-252.3
Delta F(Hz)	-65.4	-150.4	-306.9
	-54.5	-179.4	-282.6
	-53.2	-191.9	-272.4
Mean response (Hz)	-63.2	-172.8	-274.1
Standard deviations	5.7	19.4	22.4
RSD	9.1%	11.2%	8.2%

Protein resistance and glucose responding of the CNT-PEG-hydrogel

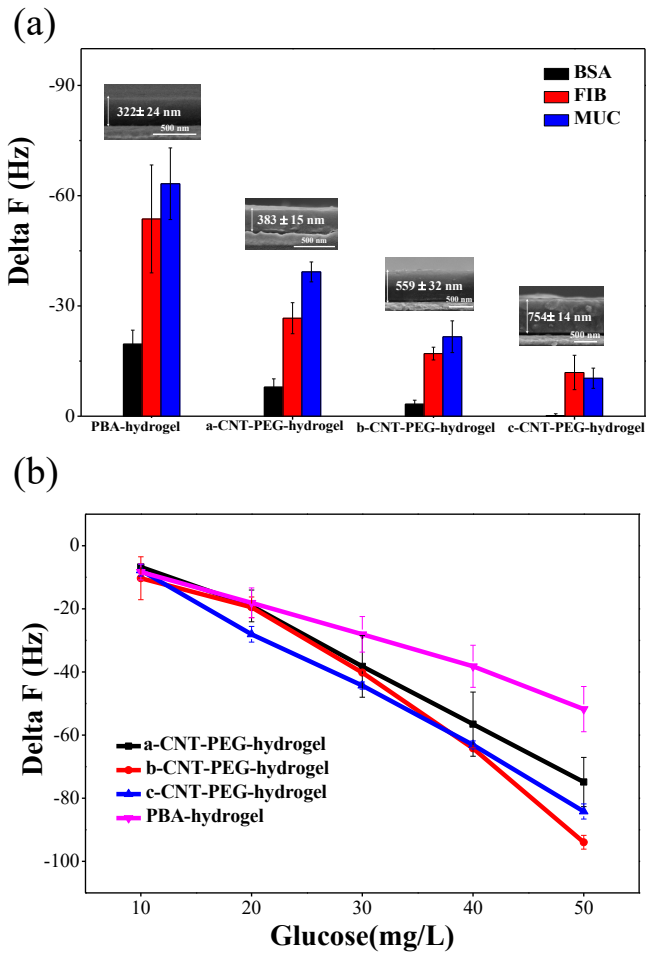

Fig. S5 (a) Adsorption of BSA (500 mg/L), MUC (500 mg/L), FIB (500 mg/L) on the CNT-PEG-hydrogel film at different thickness. (b) Response to glucose (10-50 mg/L) of the CNT-PEG-hydrogel film at different thickness.

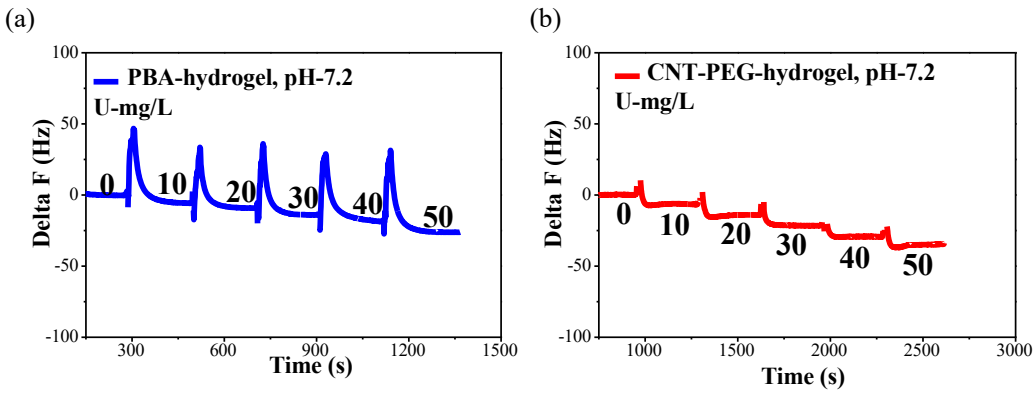

Fig. S6 (a) Response of glucose in the PBS (pH = 7.2) a by the PBA-hydrogel film. (b) Response of glucose in the PBS (pH = 7.2) a by the CNT-PEG-hydrogel film.

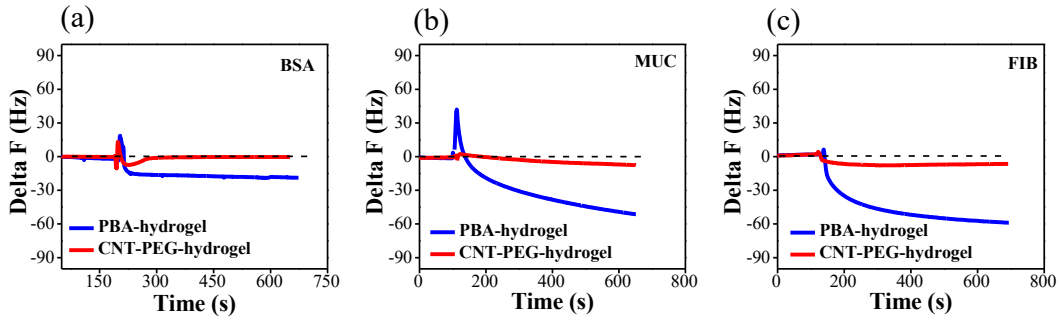

Fig. S7 Adsorption of BSA (500 mg/L) (a), MUC (500 mg/L) (b), FIB (500 mg/L) (c) on the PBA-hydrogel and CNT-PEG-hydrogel film.

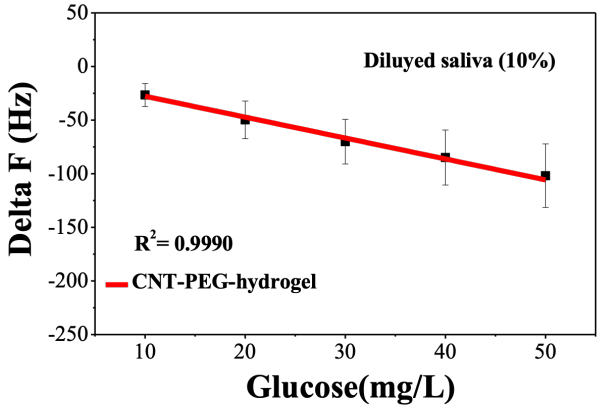

Fig. S8 Relationship between frequency shift and glucose concentration in the diluted saliva (10%).

The reproducibility of quartz crystal

Regeneration ability is an important feature of the superior performance of QCM sensor. It can effectively reduce the cost of quartz crystal. To achieve the regeneration of the quartz crystal, it is necessary to peel the CNT-PEG-hydrogel off the quartz crystal through the appropriate way. In this experiment, to realize the regeneration of quartz crystal, we washed quartz crystal in piranha solution (VH_2SO_4: VH_2O_2 = 7:3) for ultrasonic cleaning 10 min, and then washed with deionized water for 5 min. As shown in **Fig. S9**, we found that the frequency shift of quartz crystal can be controlled within 50 Hz after fifteen repeating. This result demonstrates that the quartz crystal has a good reproducibility.

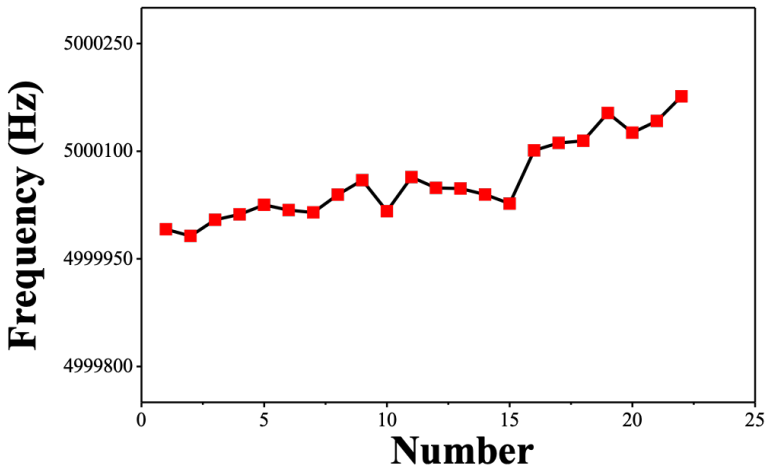

Fig. S9 The frequency shift response of the sensor after multiple regeneration

The disturbance of small molecules

The binding between the anionic boronate species and cis-diol groups of glucose molecules is covalent. Thus, the CNT-PEG-hydrogel can be specifically combined with glucose molecules. For glucose detection (100 mg/L), the absolute value of the average of frequency displacement were more than 160 Hz. While some small molecules may be absorbed on the CNT-PEG-hydrogel film-coated QCM sensors that cause the frequency shift. The frequency shift of 100 mg/L uric acid (UA), 100 mg/L L-Cysteine (L-Cys), 100 mg/L L-glutathione (GSH) and 100 creatinine (CRE) were tested. As shown in the **Table S4,** the CNT-PEG-hydrogel film-coated sensor have superior resistance to L-Cys, GSH, UA and CRE, and the absolute value of the average of frequency displacement were all less than 15 Hz. Therefore, the CNT-PEG-hydrogel had excellent selectivity for glucose detection.

Table S4. The frequency shift of small molecules and glucose on the CNT-PEG-hydrogel film-coated QCM sensor

Film	Concentration (mg/L)	Substances	The absolute value of ΔF (Hz)
CNT-PEG-hydrogel	100	Glucose	161.0
		L-Cys	9.0
		GSH	10.8
		UA	6.5
		CRE	5.4

Preparation of CNT-PEG-hydrogel films

The CNT-PEG-hydrogel coating consists of the bottom base PBA-hydrogel film and top CNT-PEG layer. Therefore, the total thickness of the composite coating was decided by the thickness of both the PBA-hydrogel film and CNT-PEG layer. The thickness of PBA-hydrogel was determined by the pressure. And the thickness of the CNT-PEG layer was determined by the concentrations of CNT-PEG suspension, spinning speed and coating time.

In our previous work, to acquire the controllable thickness of the PBA-hydrogel layer we have developed a PBA-hydrogel by UV pressing polymerization.[4] To control film thickness, a simple film pressing device was built, as shown in **Fig. S10**. The force is exerted by pressing on the handle and is directly transferred to the QCM chip via the soft rubber contact. The magnitude of the applied force is measured by the scale column. The green line of the scale column indicates the magnitude of the pressure. In view of the advantages of this synthesis method, we continue to use this method in this work.

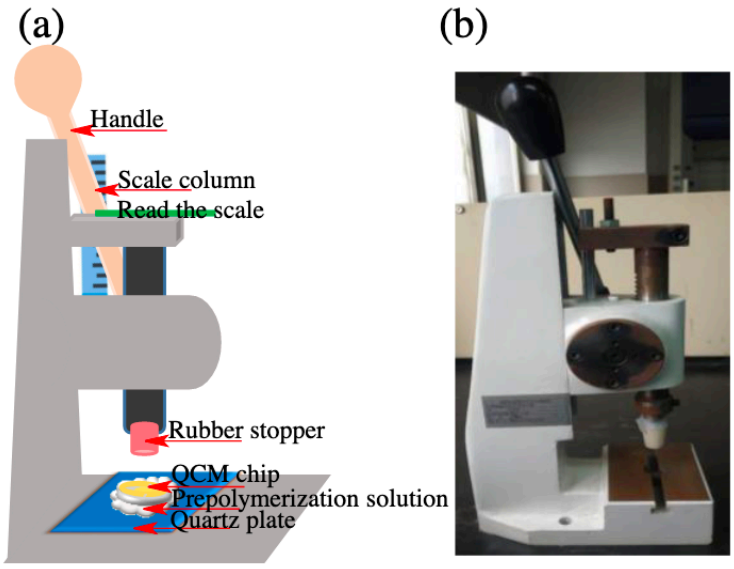

Fig. S10 Schematic diagram (a) and physical map (b) of the film pressing device.

Firstly, the thickness of PBA-hydrogel was determined by the pressure (scale column). When the scale column was 3.2 cm, the thickness of hydrogel was 962 ± 26 nm. When the scale column was of 3.7 cm, the thickness of hydrogel was 458 ± 34 nm. When the scale column was 3.9 cm, the thickness of hydrogel was 322 ± 24 nm. The standard deviation of thickness can be controlled within 40 nm. Therefore, we can obtain a certain thickness of hydrogels by UV pressing polymerization.

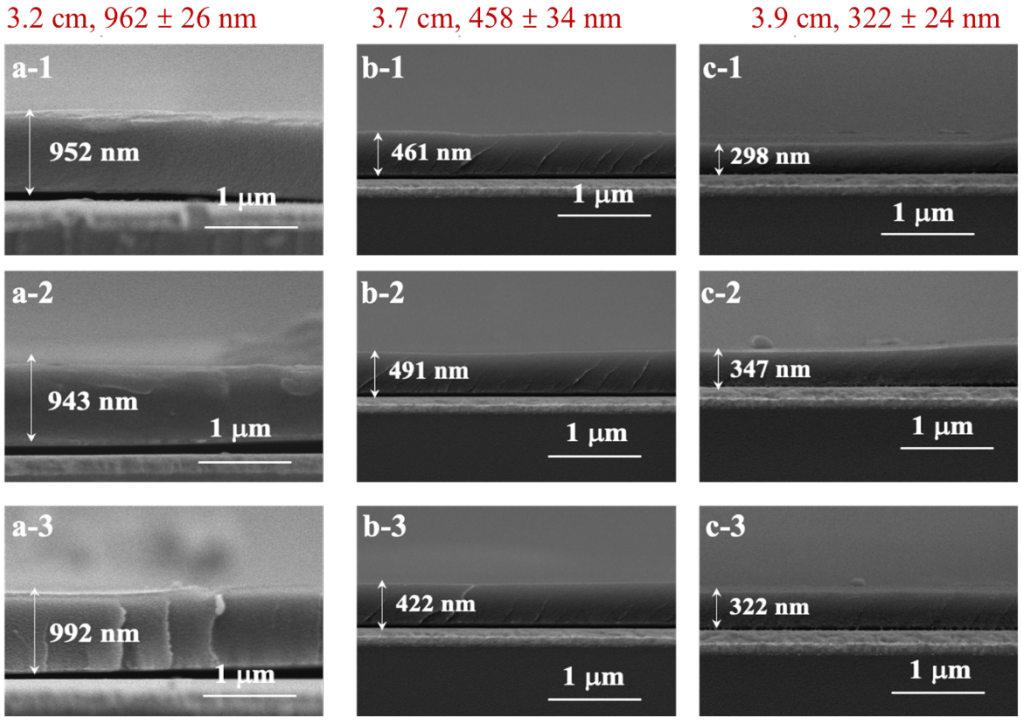

Fig. S11 SEM images of different hydrogel thickness, the scale column was 3.2 cm (a-1, a-2, a-3), the scale column was 3.7 cm (b-1, b-2, b-3), the scale column was 3.9 cm (c-1, c-2, c-3).

Secondly, under a given pressure, the thickness of CNT-PEG-hydrogel was controlled by the concentrations of CNT-PEG suspension, the speed of spin coater, and the coating time.

To acquire different thickness of the CNT-PEG-hydrogel, 250 mg/L, 500 mg/L, 1000 mg/L CNT-PEG suspensions were directly spin-coated on the PBA-hydrogel's surface, at a speed of 1000 r/min, 30 s. Finally, the CNT-PEG-hydrogel films were obtained, the thickness of CNT-PEG-hydrogel films were, 383 ± 15 nm, 559 ± 32 nm, and 754 ± 14 nm, respectively. The standard deviation of thickness can be controlled within 40 nm.

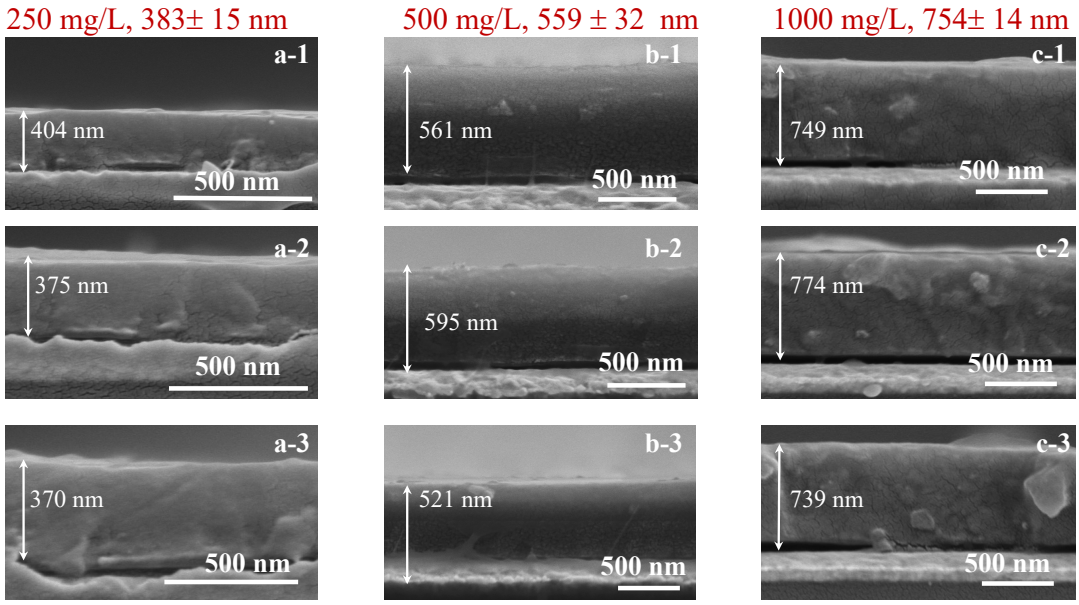

Fig. S12 SEM images of different hydrogel thickness, the concentration of CNT-PEG dispersions was 250 mg/L (a-1, a-2, a-3), 500 mg/L (b-1, b-2, b-3), 1000 mg/L (c-1, c-2, c-3), scale column was 3.9 cm.

To acquire different thickness of the CNT-PEG-hydrogel, 500 mg/L CNT-PEG suspensions were directly spin-coated on the PBA-hydrogel's surface, at a speed of 500 r/min, 1000 r/min, and 2000 r/min, respectively (coating time was 30 s). Finally, the

CNT-PEG-hydrogel films were obtained, the thickness of CNT-PEG-hydrogel films were, 903 ± 22 nm, 559 ± 37 nm, and 344 ± 16 nm, respectively. The standard deviation of thickness can be controlled within 40 nm.

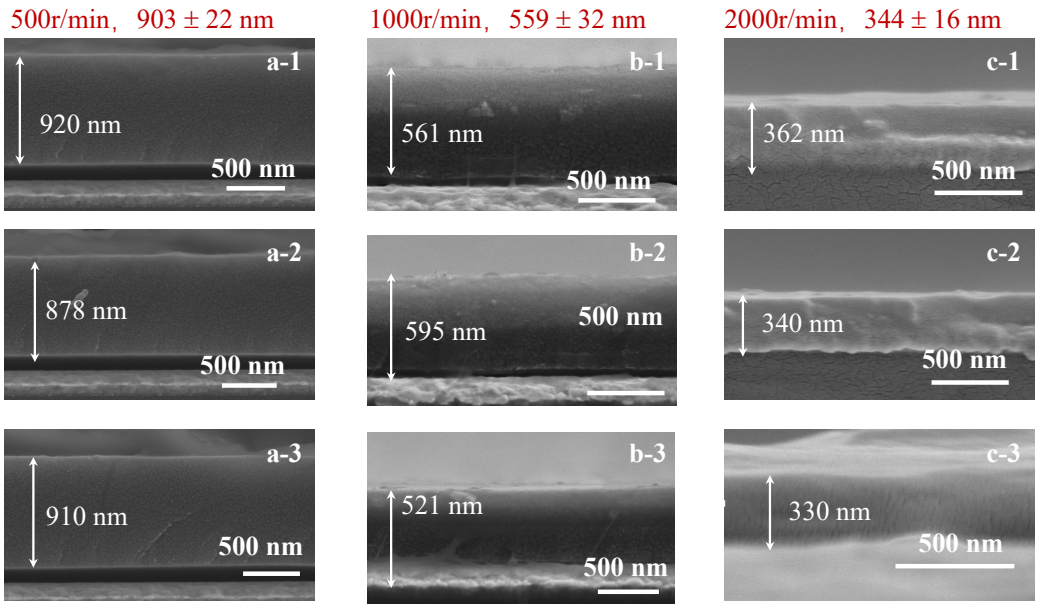

Fig. S13 SEM images of different hydrogel thickness, at a speed of 500 r/min (a-1, a-2, a-3), 1000 r/min (b-1, b-2, b-3), 2000 r/min (c-1, c-2, c-3), , scale column was 3.9 cm.

To acquire different thickness of the CNT-PEG-hydrogel, 500 mg/L CNT-PEG dispersions were directly spin-coated on the PBA-hydrogel's surface, the coating time was ,10 s, 30 s, and 50 s, respectively, at a speed of 500 r/min. Finally, the CNT-PEG-hydrogel films were obtained, the thickness of CNT-PEG-hydrogel films were, 853 ± 48 nm, 559 ± 32 nm, and 434 ± 54 nm, respectively. The standard deviation of thickness can be controlled within 60 nm.

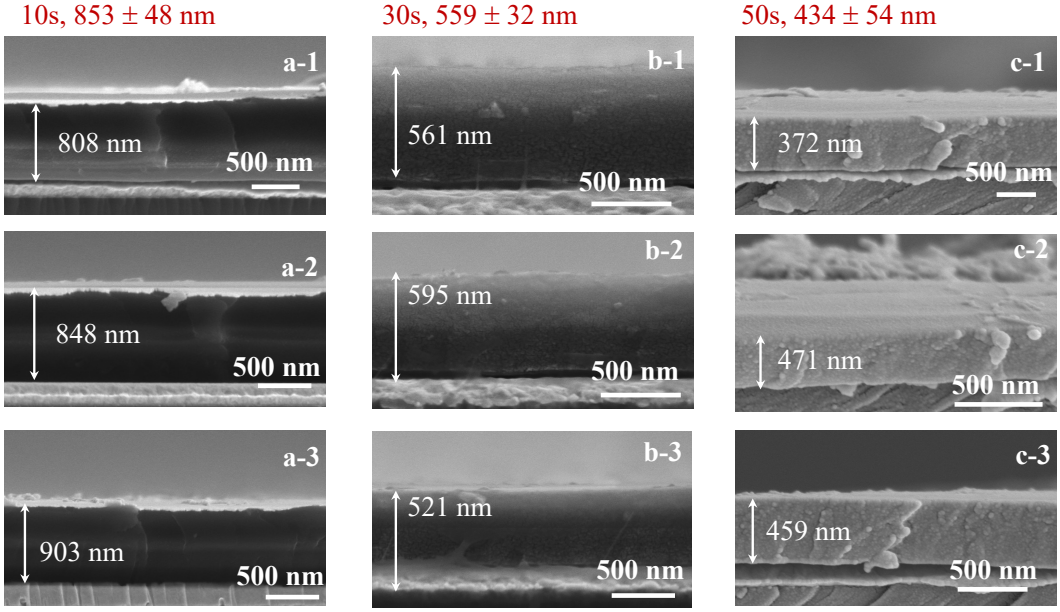

Fig. S14 SEM images of different hydrogel thickness, the coating time was 10 s (a-1, a-2, a-3), 30 s (b-1, b-2, b-3), and 50 s (c-1, c-2, c-3), scale column was 3.9 cm..

Glucose responding in the different samples

To evaluate the feasibility of the CNT-PEG-hydrogel film in response to glucose in different saliva samples,10 mg/L, 20 mg/L, 30 mg/L, 40 mg/L, 50 mg/L glucose was spiked into the samples 1, sample 2, sample 3, sample 4, sample 5, respectively (V Mixed saliva : V pH-7.5 PBS = 9:1). The relevant coefficient between glucose concentration and ΔF was $R^2 = 0.9825$."

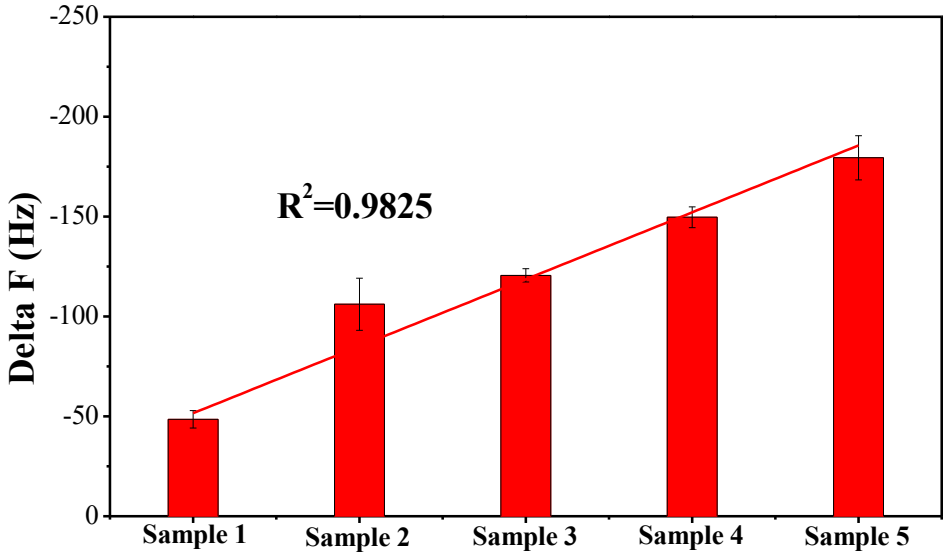

Fig. S15 Relationship between frequency shift and glucose concentration in the different saliva samples (10%).

Comparison of analytical properties of the glucose sensor

QCM sensors have been employed as a highly sensitive mass detector with accuracy up to the level of nanogram. They are widely used for probing solution-surface interfaces of a wide range of biopolymers involved in bio-recognition processes. They can transduce a biological recognition event into a measurable signal (response frequency, ΔF). Molecular recognition events at the crystal surface are instantaneously reflected in the frequency response without any external reagent/chemical for labelling, resulting in a short detection time. Even if a target analyte does not have any pronounced optical, electrochemical, or other functionalities, it still can be recognized by QCM sensors.

As shown in the **Table S5**, QCM sensor have been compared with other technologies. At present, most glucose sensors are mainly based on paper-strip or electrochemical sensor. The glucose-sensitive materials of the paper-strip and electrochemical glucose sensors are mainly focused on enzymes, such as, hexokinase, glucose oxidase (GO), and glucose-1-dehydrogenase. They have been successfully applied to measure the glucose concentration in human blood. However, they are often

difficult to reuse, which can be influenced by many factors, such as temperature, pH, and the presence of detergents. Moreover, paper-based biosensors often have low sensitivity and difficult to achieve quantitative glucose detection. For example, Soni developed a paper-based glucose sensor that can be applied to detect saliva glucose at range of 90-13500 mg/L glucose within 45 s, but the LOD value of 222 mg/L. Some electrochemical glucose sensors are based on a variety of no-enzyme materials ranging from platinum, gold, metal alloys/adatom, non-precious transition metal/metal oxides to glucose-specific organic materials, they hold the potential for regeneration. When the electrochemical glucose sensors are applied for glucose detection in real sample (such as serum, saliva), some proteins may bind nonspecifically and interfere or inhibit glucose-responsive materials/glucose interactions, thus produce false positive assay results. Also, they also have the drawback of poor selectivity, caused by surface poisoning from adsorbed intermediates (such as protein) and chloride.[4] Moreover, major drawbacks of the electrochemical sensors are involvement of complex procedures and costly reagents in sensor fabrication. SPR sensors have been designed for glucose detection, but compared with the QCM sensor, SRR sensor is expensive, hard to regenerate the sensor chip under conditions that do not denature the immobilized probe. Moreover, the complexity and noise signals of SPR sensors also limited its clinical diagnosis[11].

It should be noted that glucose-sensitive materials are the key factors to determine the properties of QCM glucose sensor. The phenylboronic acid (PBA) is often used as the sensing materials for QCM glucose sensor, and has excellent stability, durability, recoverability, and low cost compared with enzyme-based glucose sensor. Therefore, considering the advantages of QCM techniques and PBA-hydrogel, we developed a novel CNT-PEG-hydrogel film that enhanced the antifouling and sensitivity of the glucose detection. Moreover, CNT-PEG-hydrogel can be stored in the room temperature, which avoid the harsh storage condition of enzyme-based glucose sensors. Also, these excellent performances (such as antifouling, glucose sensitivity and simple

storage condition) demonstrates that the proposed QCM sensor can potentially be applied to detect glucose in complex biological samples such as saliva.

Table S5 Comparison of analytical properties of the glucose sensor

Detection method	Sensing-materials	pH	Range and limit (mg/L)	Time	Matrix	Ref
Electrochemical sensor	Co@Pt NPs	7.0	180-5400, 54	—	PBS	5
	BH-Ag/Pt NPs	3.0-10.0	180-2160, 2.34	—	PBS	6
	[Mn2(H2O)2]·2DMF	—	0.36-360, 0.018	—	0.1M NaOH	7
Optical	GOx-QDs	—	0.018-3.6, 0.00306	60 min	1/1200 Serum	8
	GOx	—	0 – 360, 0.09	30 min	10% Serum	9
	AgNC–GOx/Ag+-FP	—	9-900, 9	2 h	Cells	10
SPR	PDADMAC/GO*x*	7.0	1800-9000, —	5 min	PBS	11
	PBA	5.0	54-3600, 54	6 min	PBS	12
Paper	GOx-HPR	6.0-7.0	54-180, 6.858	30 min	Serum	13
	GOx	—	90-13500, 222	45 s	Saliva	14
	GOx	7.0	500-5400, 246	20 s	Saliva	15
EFT	PBA	7.4	18-7200, 9	8 min	PBS	16
QCM	CP	7.4	1.8- 3600	30 min	10% Serum	1
	ConA	—	1.8-1350, 0.9	—	H2O	17

PBA	7.4-9.0	18-4500, 18	30 min	PBS	[18]
PBA	7.0, 9.0	180-9000, 90	30 min	PBS	[19]
PBA	7.5	1-36, 1	5 min	PBS	[20]
PBA	7.3-7.8	10-50, 10	2 min	10% Saliva	[21]
PBA	6.8-7.5	10-50, 0.5	5 min	10% Saliva	Our work

References

1. C. Li, X. Chen, F. Y. Zhang, X. X. He, G. Z. Fang, J. F. Liu and S. Wang, *Analytical Chemistry*, 2017, **89**, 10431-10438.
2. J. Wang, Z. Wang, J. Yu, A. R. Kahkoska, J. B. Buse and Z. Gu, *Adv Mater*, 2020, **32**, e1902004.
3. C. Zhang, M. Losego and P. V. Braun, *Chem Mater*, 2013, **25**, 3239-3250.
4. Q. Dou, Z. Zhang, Y. Wang, S. Wang, D. Hu, Z. Zhao, H. Liu and Q. Dai, *ACS Applied Materials & Interfaces*, 2020, **12**, 34190-34197.
5. H. Mei, W. Wu, B. Yu, Y. Li, H. Wu, S. Wang and Q. Xia, *Microchimica Acta*, 2015, **182**, 1869-1875.
6. D. Ma, X. Tang, M. Guo, H. Lu and X. Xu, *Ionics*, 2014, **21**, 1417-1426.
7. Arum, Kim, Siddharthya, Mujumdar, Ronald and Siegel, *Chemosensors*, 2013, **2**, 1-1.
8. G. Mao, Y. Ma, G. Wu, M. Du, S. Tian, S. Huang, X. Ji and Z. He, *Anal Chem*, 2021, **93**, 777-783.
9. H. He, X. Xu, H. Wu and Y. Jin, *Advanced Materials*, 2012, **24**, 1736-1740.
10. S. Jiang, Y. Zhang, Y. Yang, Y. Huang, G. Ma, Y. Luo, P. Huang and J. Lin, *ACS Appl Mater Interfaces*, 2019, **11**, 10554-10558.
11. A. Baba, P. Taranekar, R. R. Ponnapati, W. Knoll and R. C. Advincula, *ACS Appl Mater Interfaces*, 2010, **2**, 2347-2354.
12. A. Stephenson-Brown, H. C. Wang, P. Iqbal, J. A. Preece, Y. Long, J. S. Fossey, T. D. James and P. M. Mendes, *Analyst*, 2013, **138**, 7140-7145.
13. X. Chen, J. Chen, F. Wang, X. Xiang, M. Luo, X. Ji and Z. He, *Biosens Bioelectron*, 2012, **35**, 363-368.
14. A. Soni and S. K. Jha, *Biosens Bioelectron*, 2015, **67**, 763-768.
15. A. Soni and S. K. Jha, *Anal Chim Acta*, 2017, **996**, 54-63.
16. T. Kajisa and T. Sakata, *Sci Technol Adv Mat*, 2017, **18**, 26-33.

17. D. Tang, Q. Li, J. Tang, B. Su and G. Chen, *Anal Chim Acta*, 2011, **686**, 144-149.
18. N. Fortin and H. A. Klok, *ACS Appl Mater Interfaces*, 2015, **7**, 4631-4640.
19. P.-C. Huang, M.-Y. Shen, H.-h. Yu, S.-C. Wei and S.-C. Luo, *ACS Applied Bio Materials*, 2018, **1**, 160-167.
20. Z. Zhang, Q. Dou, S. Wang, D. Hu, X. Guo, B. Liao, Z. Zhao, H. Liu and Q. Dai, *Journal of Materials Chemistry C*, 2020, **8**, 9655-9662.
21. Z. F. Zhang, Q. Dou, S. W. Wang, D. B. Hu, B. Yang, Z. P. Zhao, H. L. Liu and Q. Dai, *Nanoscale*, 2020, **12**, 22787-22797.